

## Growth-sector dependence of morphological, structural and optical features in boron-doped HPHT diamond crystals

V.V. Strelchuk<sup>1</sup>, A.S. Nikolenko<sup>1</sup>, P.M. Lytvyn<sup>1</sup>, S.O. Ivakhnenko<sup>2</sup>, T.V. Kovalenko<sup>2</sup>, I.M. Danylenko<sup>1</sup>, S.V. Malyuta<sup>3</sup>

<sup>1</sup>V. Lashkaryov Institute of Semiconductor Physics, NAS of Ukraine

41, prosp. Nauky, 03680 Kyiv, Ukraine

<sup>2</sup>V. Bakul Institute for Superhard Materials, NAS of Ukraine

2, Avtozavodska str., 04074 Kyiv, Ukraine

<sup>3</sup>National Technical University of Ukraine "Igor Sikorsky Kyiv Polytechnic Institute"

37, prosp. Peremohy, 03056 Kyiv, Ukraine

E-mail: viktor.strelchuk@ccu-semicond.net, phone/fax: +38 (044) 525 64 73

**Abstract.** Semiconducting boron-doped diamond single crystals of cubo-octahedral habit with prevalent development of octahedron {111} faces and insignificant area of cube {001}, rhombo-dodecahedron {110} and tetragon-trioctahedron {311} faces were obtained using solution-melt crystallization at high pressure 6.5 GPa and temperatures 1380...1420 °C. Using the Fe-Al solvent, which allows controlled incorporation of boron dopant between  $2 \cdot 10^{-4}$ ... $10^{-2}$  at.% made it possible to vary the electro-physical properties of the crystals. Methods of micro-photogrammetry, atomic force microscopy, and micro-Raman spectroscopy were applied to reveal sectoral inhomogeneity of impurity composition and morphology of different crystal faces. The obtained crystals were shown to have high structural perfection and boron concentration ranging approximately from  $1 \cdot 10^{17}$  up to  $7 \cdot 10^{18}$  cm<sup>-3</sup>. An increase in boron concentration increases the area of {111} faces relatively to the total crystal area. Nanoscale morphological features like growth terraces, step-bunching, dendrite-like nanostructures, columnar substructures, negative growth pyramids on different crystal faces are shown to reflect peculiarities of carbon dissolution at high pressures and temperatures. The changes in the crystals' habit and surface morphology are discussed in relation to inhomogeneous variation of thermodynamic conditions of crystal growth and dissolution at different boron concentrations.

**Keywords:** boron doped HPHT diamond, Raman spectroscopy, AFM microscopy, micro-photogrammetry.

<https://doi.org/10.15407/spqeo24.03.261>

PACS 68.37.Ps, 74.25.nd, 78.30.Am, 81.05.ug, 91.10.Lh

Manuscript received 20.05.21; revised version received 13.07.21; accepted for publication 18.08.21; published online 26.08.21.

### 1. Introduction

The search for new functional semiconductor materials for electronic devices, which has taken place over the world in recent decades, has shown particular interest to diamond [1, 2], caused by its unique electro-physical properties, namely: the high critical electric field, high mobility of holes and electrons, wide band gap, which can be changed by doping in the growth process. These properties are promising for the development of power, high-frequency, and radiation-resistant electronic devices. To date, diamond-based transistors [3, 4], diodes [5], detectors of X-ray and nuclear radiation, lasers,

optoelectronic switches, and photodetectors have been already demonstrated [1].

One obstacle towards the further development of diamond-based electronics is the lack of high-quality structurally perfect diamond substrates with a uniform defect-impurity composition throughout their bulk. The most appropriate for the needs of solid-state electronics are the substrates based on single-sector diamond plates with a uniform distribution of dopants. In particular, for the development of diamond Schottky diodes with vertical charge transport, electrically conductive diamond substrates of a large size and low defect density are required [6].

The problem to obtain semiconducting diamond material is related to a limited choice of impurities that form acceptor (B: 0.37 eV) or donor (N: 1.7 eV, P: 0.57 eV) energy levels in the band gap of the diamond. Boron is the most suitable acceptor impurity to get *p*-type semiconducting diamond, whereas nitrogen is the main compensating donor impurity.

Today, the temperature gradient method allows to grow high-quality large-size diamond crystals under high pressure and high temperature (HPHT) [7]. Doping of HPHT-diamonds is carried out by adding boron-containing components to the growth systems [8]. Optimization of structural elements of growth cells and thermodynamic growth conditions makes it possible to reduce the probability of capturing the inclusions from the growth medium by the crystal, and the use of additive components that change the thermodynamic activity and incorporation of nitrogen and boron into the diamond crystal (Ti, Al, Zr, Mg) makes it possible to optimize their concentrations in the grown diamond crystals.

Incorporating donor and acceptor impurities into the diamond crystal lattice depends on the composition of the used solvent. Semiconductor diamonds with a reduced nitrogen content and an increased boron content were obtained using carbon solvents based on Fe-Al, Fe-Mg-Al, and Fe-Co-Al-Mg [9]. Recently, using Mg in the growth systems made it possible to produce type IIb diamond crystals meeting the basic requirements of solid-state electronics in terms of their electrical properties [10]; it is shown that the growth rate of these crystals can be an order of magnitude higher in comparison with the solvents based on transition metals. It was found that an increase in the Mg content and growth temperature in the systems based on Fe-C and Fe-Al-C leads to a significant increase in the boron concentration in diamond crystals [11].

Difference in incorporating boron and the complex nature of the growth and defect-formation processes for different crystallographic faces of HPHT-diamond significantly affect their electrical properties; the highest content of nitrogen and boron is expected for octahedral {111} and trigon-trioctahedral {113} growth sectors [12–15]. The relevant distribution of temperature conditions can control the effect of inhomogeneous incorporation of boron impurities into various growth sectors of diamond during its growth [16].

Raman spectroscopy enables to study the structural and phonon properties of diamond depending on doping and crystallization conditions [5, 6]. The most intense feature in the first-order Raman spectrum of diamond is the  $F_{2g}$  mode of the Brillouin zone center stretching vibrations registered close to  $1332\text{ cm}^{-1}$ . Doping the diamond with boron impurities leads to broadening and low-frequency shift of the  $F_{2g}$ -band [9, 19], as well as to the appearance in the spectra of a series of additional vibration bands in the region below  $1200\text{ cm}^{-1}$  increasing in intensity with boron content [19–21]. Defect-induced activation of density of phonon states (DOS) and local vibration modes of boron in diamond lattice cause the nature of the additional Raman bands [19].

It was previously shown that HPHT-diamond crystals grown in Fe-Co-Mg-C systems [10] have several unique properties of micro- and macro-morphology, as well as internal structure. It should be noted that studies of faces' micro-morphology and growth accessories at different stages of crystal growth are quite informative regarding the features of crystallization processes. These features of growth, especially at early stages, can lead to formation of unwanted inclusions and defects in the crystal's bulk limiting its usability. In particular, elongated laminar formations are observed in the {111} and {100} growth sectors with a transition to parallel shading on the {110} and {311} growth sectors for diamonds grown in the Fe-Co-Mg-C system, which is related with the layer-by-layer mechanism of the {111} and {100} growth sectors and the passive growth of the {110} and {311} sectors [22]; in the micro-relief, both growth and dissolution figures are observed as typical for diamond cavities (pits) of a triangular and hexagonal shape on the faces of an octahedron, and of a quadrangular shape on the faces of a cube; elements of dendritic growth may also be present.

This work, using the methods of atomic force microscopy (AFM) and micro-Raman spectroscopy, is aimed at studying the influence of sectoral inhomogeneity of boron impurity incorporation on the structural and morphological properties of growth faces of HPHT-diamond crystals grown in the Fe-Al-C-B system. Changes in the crystal habit and nanoscale surface morphology of different crystal faces have been discussed in relation to the possibility of a non-uniform change in thermodynamic conditions and the peculiarities of crystal growth-dissolution processes depending on the boron impurity concentration in the growth medium.

## 2. Experimental details

Different levels the boron doping of diamond crystals were achieved with the growth by using the temperature gradient method at  $T = 1380\text{--}1420\text{ }^\circ\text{C}$ ,  $P = 6.5\text{ GPa}$  in a preliminarily prepared Fe-Al-B-C growth system with seed crystals having the size close to  $0.4\times 0.4\text{ mm}$  and cubic face to initiate the growth. The size of the cubic face, from which the crystal growth began, was  $\sim 100\times 100\text{ }\mu\text{m}$ .

Fig. 1a shows selected for the study three typical single crystals of HPHT diamond of cubo-octahedral habit, designated as the crystals A, B, and C. These crystals have well-developed {111}, {100} faces, much smaller {110} and {113} ones, and corresponding growth sectors in their volume [16]. The samples A and B were grown for 96 and 120 hours, respectively, with addition of a certain amount of boron additives; the masses and volumes of crystals A, B, C were 0.585 ct and  $\sim 33\text{ mm}^3$ , 0.440 ct and  $\sim 21\text{ mm}^3$  and 0.360 ct and  $\sim 19\text{ mm}^3$ , respectively.

The geometric shape (habit) of the selected diamond single crystals was investigated using micro-photogrammetry [23–25], and a digital 3D models of each crystal were constructed. Photogrammetry allows

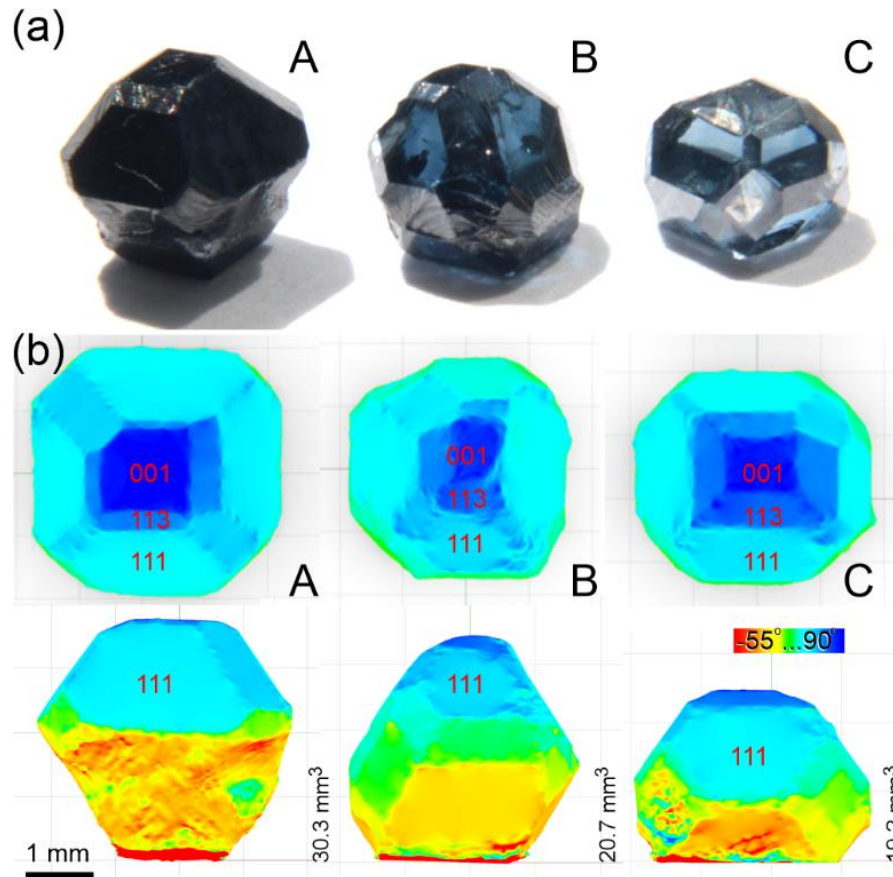


**Fig. 1.** (a) Images of diamond single crystals of octahedral and octahedron-tetragon trioctahedron-cubic habit, grown with addition of boron to the growth medium; (b) 3D scans of the crystals obtained using micro-photogrammetry with the corresponding maps of the surface normals angles for the crystallographic facets of the diamond crystal and their corresponding volumes.

determining the spatial coordinates of the object surface by using several images of the object obtained under different angles. Photogrammetry of the diamond crystals A, B and C was carried out being based on 200 images of each crystal, which were recorded with a digital camera having a multi-lens macro-objective calibrated with account of spatial distortion. The image pixel size was  $4.5 \mu\text{m}$ . The correspondence of the digital 3D models to real crystals was controlled using micrometry. The processing and analysis of the obtained images of diamond crystals were carried out using the Metashape and Meshlab software packages.

The nanoscale relief of the crystal faces, corresponding to  $\{001\}$ ,  $\{111\}$ , and  $\{113\}$  growth sectors, was studied with scanning atomic force microscopy by using a Dimension 3000 NanoScopeIIIa probe microscope. The measurements were carried out with silicon probes with a nominal tip radius of 10 nm in the tapping contact mode.

The distribution of boron dopant in  $\{001\}$ ,  $\{101\}$ ,  $\{113\}$ ,  $\{111\}$  growth sectors of the HPHT-diamond single crystals was studied using Raman micro-spectroscopy. Raman spectra were measured at room temperature in the backscattering geometry from  $\{001\}$ ,

$\{111\}$ ,  $\{101\}$ ,  $\{113\}$  facets of diamond crystals by using a Horiba Jobin-Yvon T-64000 spectrometer equipped with electrically cooled Si CCD detector and Olympus BX41 microscope. The line of Ar-Kr Stabilite 2018 RM Spectra Physics laser with the wavelength 488 nm was used for excitation.

## 2. Results and discussion

The general view of the HPHT diamond crystals selected for the study is shown in Fig. 1a. The crystals have well-developed flat facets; they differ in transparency, varying from the almost opaque gray-blue crystal A to the transparent light-blue crystal C; different degrees of blue color correspond to the varying boron content. It should be noted that the blue color of diamond crystals is due to the photoionization continuum of boron impurity, which starts in the infrared region from approximately  $3.3 \mu\text{m}$  and extends into the visible region, causing absorption in the yellow-red spectral range. No inclusions of metallic solvent or pronounced internal macro-growth defects are observed in the crystals. The shape of the crystals deviates from the symmetric one;

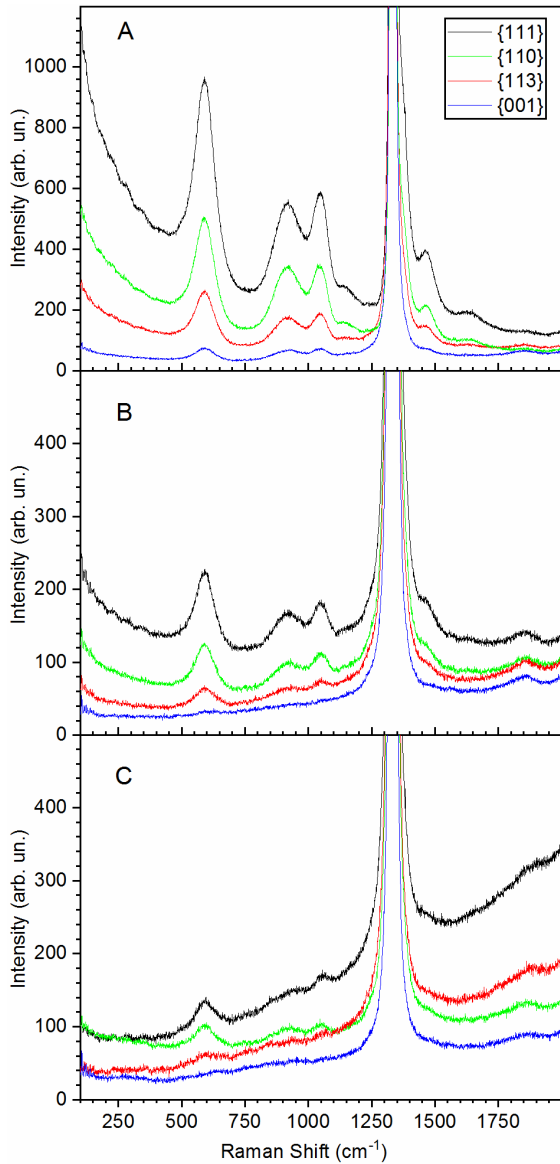


**Fig. 2.** Raman spectra of the studied HPHT diamond single crystals measured in the backscattering geometry from the {001}, {111}, {110}, and {113} faces. The spectra are normalized to the intensity of diamond  $F_{2g}$  phonon band.  $T = 300$  K.  $\lambda_{exc} = 488$  nm.

crystallographically equivalent facets have different degrees of development. The surface dissolution in the lower part of the crystals are observed, especially for the crystals A and B (Fig. 1).

The features of boron content distribution in different growth sectors of the HPHT diamond crystals were studied with micro-Raman spectroscopy by using the respective spectra obtained for different faces of the studied crystals (Fig. 2). An intense  $F_{2g}$  vibration band of diamond with the frequency close to  $1332\text{ cm}^{-1}$  and the half-width approximately  $2.0\text{ cm}^{-1}$  is caused by first-order scattering by optical phonons at the Brillouin zone center. Wide additional bands registered in the low-frequency spectral range at  $588$ ,  $920$ , and  $1046\text{ cm}^{-1}$  can

be related to incorporating boron impurities into the diamond lattice. Similar Raman spectra were observed for the type IIb HPHT diamonds with the boron concentration from  $1 \cdot 10^{17}$  up to  $7 \cdot 10^{18}\text{ cm}^{-3}$  [19], while the change in the relative intensity of the observed additional bands reflects the change in the boron concentration, which is the lowest for the crystal C and highest for the crystal A.

Fig. 3a shows the relative intensity of the most pronounced phonon band at  $588\text{ cm}^{-1}$ , caused by boron impurity. Relative intensity of this band gradually decreases in the sequence  $\{111\} \rightarrow \{110\} \rightarrow \{113\} \rightarrow \{001\}$ , which reflects variation of boron content in the corresponding growth sectors of the studied crystals; this agrees with previous studies [12, 13, 15]. Note that boron content for the {001} growth sector of weakly doped crystals B and C is lower than the detection limit of Raman spectroscopy in our case. The sectoral inhomogeneity of boron content is also reflected by the change in the full-width at half-maximum (FWHM) of diamond  $F_{2g}$ -band (Fig. 3b), which is almost unchanged and equals  $1.96\text{ cm}^{-1}$  for the crystals C and B, and gradually increases for the crystal A from  $1.94$  to  $2.13\text{ cm}^{-1}$  (Table) for different faces in the sequence  $\{001\} \rightarrow \{113\} \rightarrow \{110\} \rightarrow \{111\}$ .

This effect can be related to the Fano resonance between optical phonons  $\omega_{opt}$  and the electron continuum of boron-doped diamond [9, 26]. Note that the spectral position of the  $F_{2g}$  band in all the spectra is almost unchanged and remains near  $1333.0\text{ cm}^{-1}$  (Table).

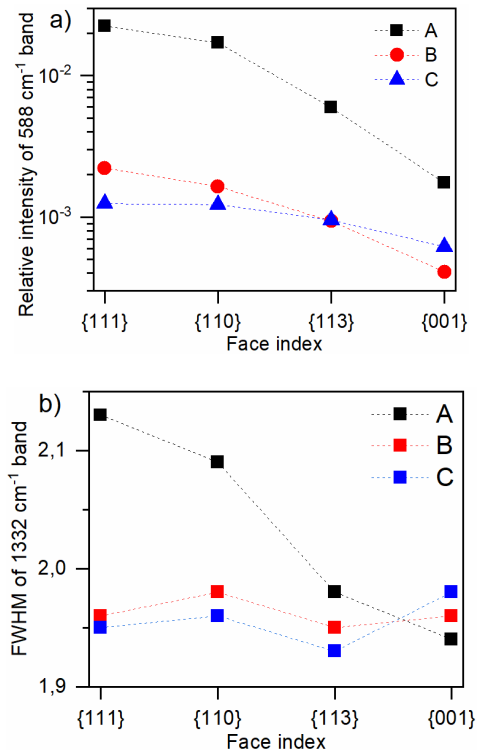


**Fig. 3.** The relative intensity of the phonon band at  $588\text{ cm}^{-1}$  (a) and full-width at half-maximum of  $F_{2g}$  phonon band (b) for different faces of the studied HPHT diamond single crystals.



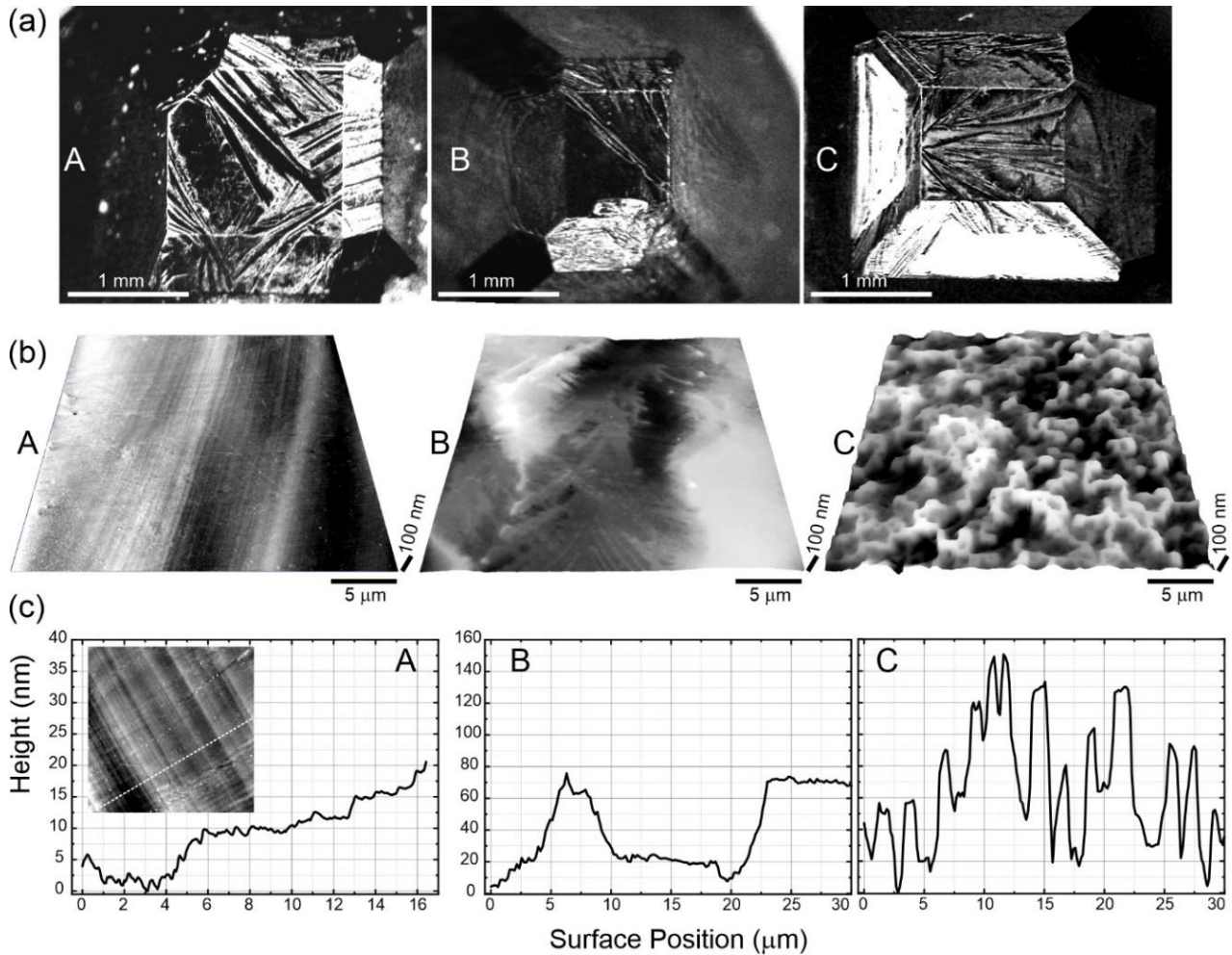


**Fig. 5.** Micro- and nano-morphological features of the growth figures of the  $\{001\}$  facet for the crystals A, B, and C: optical images (a), 3D AFM images of nano-relief of characteristic regions (b), profiles of the facet relief from AFM data (c).

this type are characterized by layer-by-layer growth of the main shaping facets (growth sectors)  $\{001\}$  and  $\{111\}$  with gradual filling the volume between them with low-index growth facets  $\{113\}$  and  $\{115\}$ . However, along with layer-by-layer growth, desorption of adatoms and dissolution (etching) of the growth surface are significant.

Figs 5 to 7 show a comparison of the low-index growth surfaces of crystals A, B, C. Lamellar growth bands passing through the facets of different indices are observed on all the crystals in the optical microscopy images; these bands arise because of the specific character of solidification inherent to the liquid growth medium [22]. In homogeneous areas of these bands, the nanoscale relief was studied using AFM microscopy. The  $\{001\}$  face of crystal A is characterized by a clearly pronounced layer-by-layer nature of the solidification process; elongated, parallel single growth terraces with a

step height of about 3 nm and their step-bunching with formation of steps up to 10 nm are observed (Figs 5b and 5c). On the  $\{001\}$  facet of crystal B, these bands are no longer observed; pits and plateaus are formed with lateral dimensions of several tens of micrometers and with height differences of the order of 70 nm.

Formation of dendrite-like nanostructures (Fig. 5b) at the last stages of crystallization is also typical. Somewhat unexpected is observation of columnar substructures on the surface of the  $\{001\}$  facet of crystal C (Fig. 5b). The substructures show an ordered texture with a clear reference to the selected crystallographic directions. The difference in the heights of these structures is 100...150 nm. Considering the duration of growth process and the relatively low growth rate of this facet, formation of this substructure can be associated with the significant influence of the dissolution processes (desorption, etching).

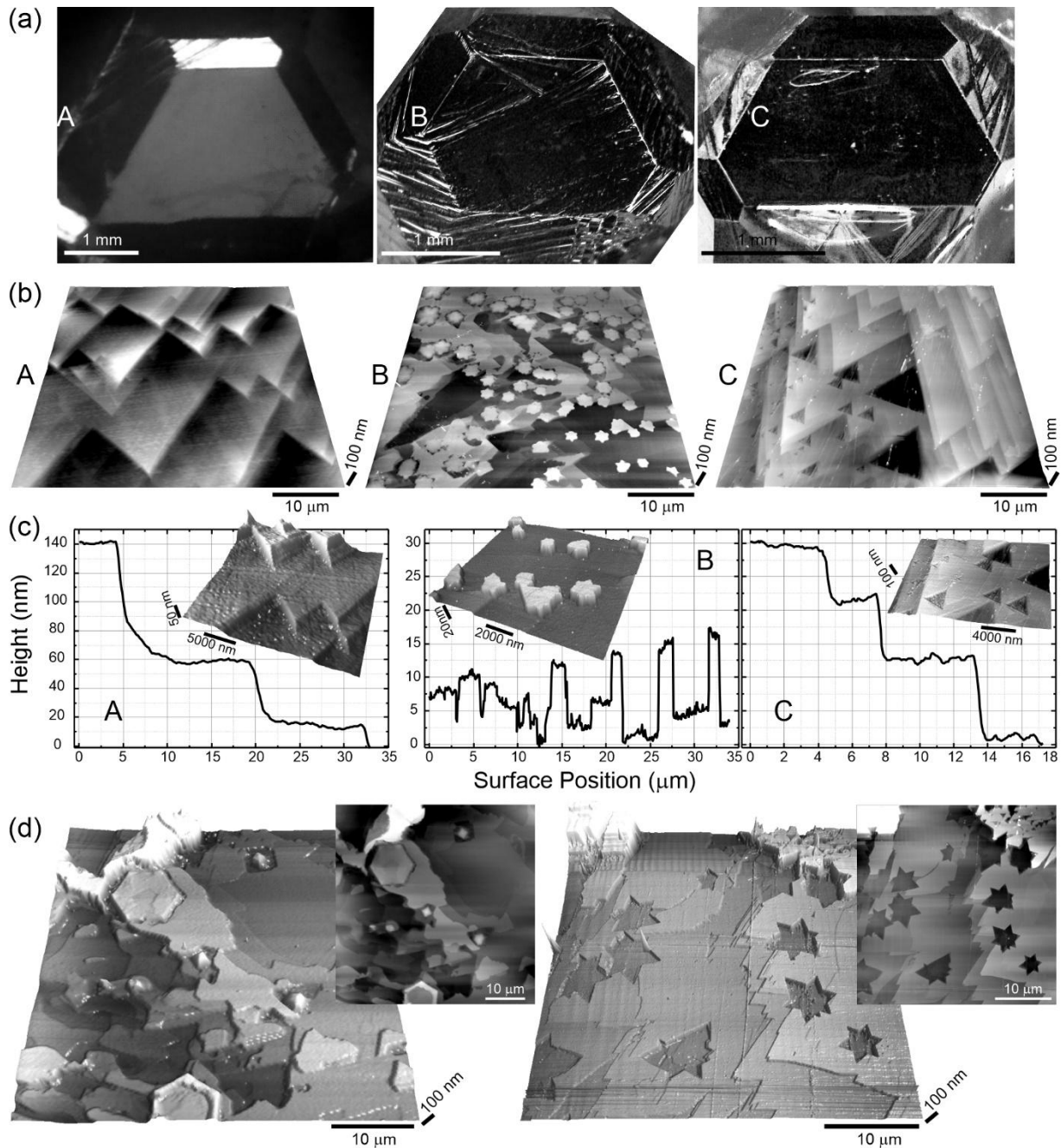


**Fig. 6.** Micro- and nano-morphological features of the growth figures of the  $\{111\}$  facet for the crystals A, B, and C: optical images (a), 3D AFM images of nano-relief of characteristic regions (b), profiles of the facet relief according to AFM measurements (c), variations of micro-defects on the surface of the crystal B (d). Insets in (c) shows enlarged fragments of AFM images (b), and insets in (c) show 2D AFM images.

Morphology of the  $\{111\}$  facets of crystals A and C is quite similar (Fig. 6b). Propagation of characteristic growth terraces as triangles with the angle  $60^\circ$  at the apex is observed. A feature of the  $\{111\}$  surface of crystal A is a significant terrace height of  $40\dots 80$  nm and the absence of growth defects on them. The crystal C is characterized by the appearance of negative growth pyramids (triangular depressions) of various sizes and a relatively

small height of the terraces close to  $10\dots 15$  nm. Typical stepped terrace profiles are shown in Fig. 6c. The crystal B is characterized by the absence of ordered growth bands and the presence of micro-defects of various shapes: from pits as pairs of opposite negative growth pyramids to the inversion of these pairs of pyramids into protrusions of 10 nm in height, as well as protrusions as squares and regular hexagons (Fig. 6d).

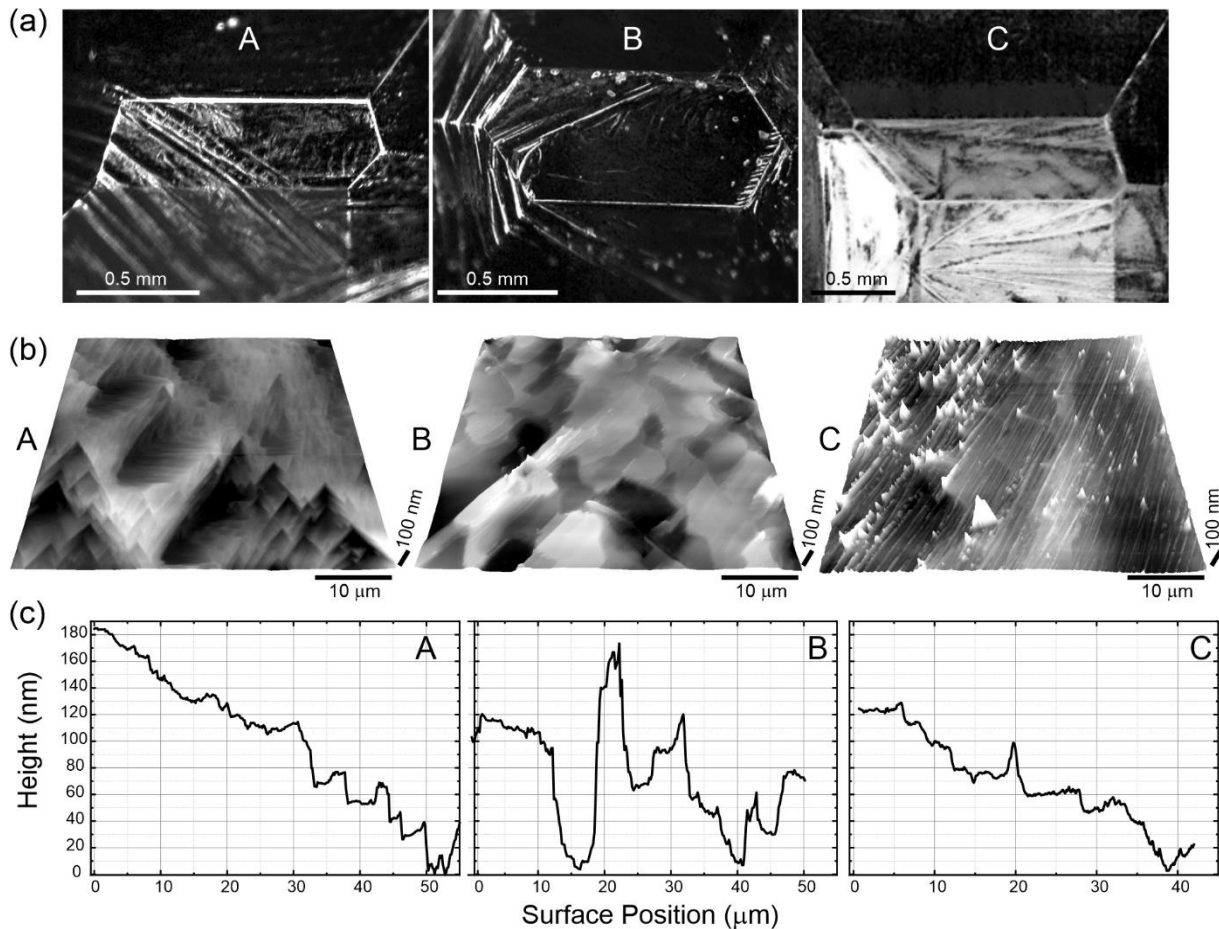


**Fig. 7.** Micro- and nano-morphological features of the growth figures of the  $\{113\}$  facets for the crystals A, B and C: optical images (a), 3D AFM images of nano-relief of characteristic regions (b), profiles of the facet's relief according to AFM measurements (c).

The characteristic transverse dimensions of these defects are  $1 \dots 10 \mu\text{m}$ , and their surface density reaches  $1.6 \cdot 10^3 \text{ cm}^{-2}$ . The origin of these defects could be associated with some contaminations and dislocations originated from impurities segregation [27].

It is difficult to distinguish any individual features on the  $\{113\}$  faces of the crystals under study. Their morphology is mostly determined by morphology of the most developed  $\{111\}$  faces. Thus, the  $\{113\}$  facets of crystal A (Fig. 7) are characterized by weakly ordered triangular growth bands with a step height of  $10 \dots 50 \text{ nm}$ . For the crystal C, we have weakly pronounced triangular growth bands with a step height of  $5 \dots 20 \text{ nm}$ . The crystal B has irregular  $\{113\}$  growth surfaces with pronounced flat deepening and plateaus with the height differences of about  $150 \text{ nm}$ .

### 3. Conclusions

The crystallization process of boron-doped  $p$ -type semiconductor diamonds, obtained at high pressures and temperatures in the region of thermodynamic stability when being grown on a seed, enables to obtain

structurally perfect faceted forms of crystals with a boron content up to  $\sim 10^{19} \text{ cm}^{-3}$ . The level of the boron dopant in the crystals can be changed by varying the crystallization conditions and introducing a greater or lesser amount of boron additives into the solvent.

An increase in boron content in the Fe-Al-B-C growth system leads to an increase in the growth rate and a change in development of diamond crystal faces; under the same growth conditions, a decrease in the concentration of boron impurities in different growth sectors in the sequence  $\{111\} \rightarrow \{110\} \rightarrow \{113\} \rightarrow \{001\}$  is observed. Highly doped diamond crystals have more pronounced development of octahedral faces and are elongated along the carbon transfer and the growth axis. There are both macro- and micro-figures of dissolution (etching) with a size of  $1 \dots 5 \mu\text{m}$  on the growth surfaces of these crystals. The growth patterns of the highly doped crystals indicate that the facet growth occurred under the uniform conditions and with insignificant desorption processes. For the  $\{001\}$  face, layer-by-layer growth is observed, while for the  $\{111\}$  and  $\{113\}$  facets, growth of this kind is accompanied by formation of growth pyramids on the surface. For the  $\{111\}$  facet of the

lightly boron doped crystals, as well as for heavily doped crystals, layer-by-layer growth with significantly lower growth pyramids is observed; the {001} facet has signs of dissolution (etching) with characteristic figures along the crystallographic directions of the crystal; the growth pyramids on the {113} crystal facet are weakly pronounced.

Considering the sectoral structure of the grown crystals, each of the growth pyramids on the facets {111}, {113} {110} and {100} has a certain amount of boron, which can differ from each other several times. In addition, the defect-impurity composition of each of the growth sectors is also significantly different. These reasons cause the use of a single-sector material to provide uniformity of the semiconducting properties of the samples. Sometimes, this material can be a diamond of the {111} sector – for example, for use as diamond semiconductor thermistors. In other cases, it is necessary to use the diamond of the growth sectors {100}, {113} and {110}. As our previous studies have shown, the most promising semiconducting material for the use in diamond-based Schottky diodes is boron-doped diamond having a defect-impurity structure of the {100} and {311} growth sectors, which is due to better electrical characteristics, in particular, higher mobility of charge carriers as compared with the {111} growth sector [28, 29].

Sufficient development of the {100} and {113} growth sectors can be ensured by varying the growth conditions and, first of all, by choosing a specific solvent composition. As our studies have shown, the use of growth systems based on the Fe-Al-B-C enables to grow semiconductor diamond single crystals with sufficiently large volumes of the {100} and {113} sectors (Fig. 1c, crystal C), these volumes can be significantly increased by increasing development of certain growth sectors and the crystal volume. Along with growing these crystals, the problem of obtaining only one-sector material arises. It is possible to solve this problem by using the developed micro-photogrammetry approach to study the crystal habit with the ability to construct their digital 3D models. Besides, visualizing the shape of the crystals grown on seeds and determining the configuration of crystal facets and edges, 3D models are of interest for determining the directions of mechanical or laser processing of crystals and localization of one-sector regions of semiconductor diamond crystals.

#### Acknowledgement

The authors are grateful to the National Research Foundation of Ukraine for financial support in the framework of the project № 2020.02/0160 “Development of new carbon solvents compositions for diamond single crystals growth in the thermodynamic stability area with a controlled content of nitrogen and boron impurities in order to create conceptual electronic devices construction”.

#### References

1. Sussmann R.S., ed. *CVD Diamond for Electronic Devices and Sensors*. John Wiley&Sons. Chichester, UK, 2009. <https://doi.org/10.1002/9780470740392>.
2. Satoshi K., Hitoshi U., Julien P., Mariko S., eds. *Power Electronics Device Applications of Diamond Semiconductors*. Elsevier, 2018. <https://doi.org/10.1016/C2016-0-03999-2>.
3. Kato H., Oyama K., Makino T. *et al.* Diamond bipolar junction transistor device with phosphorus-doped diamond base layer. *Diam. Relat. Mater.* 2012. **27–28**. P. 19–22. <https://doi.org/10.1016/j.diamond.2012.05.004>.
4. Iwasaki T., Yaita J., Kato H. *et al.* 600 V diamond junction field-effect transistors operated at 200 °C. *IEEE Electron Device Lett.* 2014. **35**. P. 241–243. <https://doi.org/10.1109/LED.2013.2294969>.
5. Volpe P.-N., Muret P., Pernot J. *et al.* High breakdown voltage Schottky diodes synthesized on *p*-type CVD diamond layer. *phys. status solidi.* 2010. **207**. P. 2088–2092. <https://doi.org/10.1002/psa.201000055>.
6. Bormashov V.S., Terentiev S.A., Buga S.G. *et al.* Thin large area vertical Schottky barrier diamond diodes with low on-resistance made by ion-beam assisted lift-off technique. *Diam. Relat. Mater.* 2017. **75**. P. 78–84. <https://doi.org/10.1016/j.diamond.2017.02.006>.
7. Lysakovskiy V.V., Novikov N.V., Ivakhnenko S.A. *et al.* Growth of structurally perfect diamond single crystals at high pressures and temperatures. Review. *J. Superhard Mater.* 2018. **40**. P. 315–324. <https://doi.org/10.3103/S1063457618050039>.
8. Wentorf R.H., Bovenkerk H.P. Preparation of semiconducting diamonds. *J. Chem. Phys.* 1962. **36**. P. 1987–1990. <https://doi.org/10.1063/1.1732815>.
9. Utyuzh A., Timofeev Y., Rakhmanina A. Effect of boron impurity on the Raman spectrum of synthetic diamond. *Inorg. Mater.* 2004. **40**. P. 926–931. <https://doi.org/10.1023/B:INMA.0000041323.35298.dd>.
10. Kovalenko T.V., Ivakhnenko S.A. Properties of diamonds seed-grown in the magnesium-carbon system. *J. Superhard Mater.* 2013. **35**. P. 131–136. <https://doi.org/10.3103/S1063457613030015>.
11. Kovalenko T.V., Ivakhnenko S.A., Lysakovskiy V.V. *et al.* Defect-and-impurity state of diamond single crystals grown in the Fe–Mg–Al–C system. *J. Superhard Mater.* 2017. **39**. P. 83–87. <https://doi.org/10.3103/S1063457617020022>.
12. Zubkov V., Solomnikova A., Koliadin A., Butler J.E. Analysis of doping anisotropy in multisectorial boron-doped HPHT diamonds. *Mater. Today Commun.* 2020. **24**. P. 100995. <https://doi.org/10.1016/j.mtcomm.2020.100995>.
13. Klepikov I.V., Koliadin A.V., Vasilev E.A. Analysis of type IIb synthetic diamond using FTIR spectrometry. *IOP Conf. Ser. Mater. Sci. Eng.* 2017. **286**. 012035. <https://doi.org/10.1088/1757-899X/286/1/012035>.

14. Howell D., Collins A.T., Loudin L.C. *et al.* Automated FTIR mapping of boron distribution in diamond. *Diam. Relat. Mater.* 2019. **96**. P. 207–215. <https://doi.org/10.1016/j.diamond.2019.02.029>.
15. Solomnikova A., Lukashkin V., Zubkov V., Kuznetsov A., Solomonov A. Carrier concentration variety over multisectoral boron-doped HPHT diamond. *Semicond. Sci. Technol.* 2020. **35**. P. 095005. <https://doi.org/10.1088/1361-6641/ab9a5f>.
16. Chepugov A., Ivakhnenko S., Garashchenko V. The study of large semiconducting boron doped single crystal diamond sectorial structure. *phys. status solidi*. 2014. **11**. P. 1431–1434. <https://doi.org/10.1002/pssc.201300633>.
17. Kim H., Vogelgesang R., Ramdas A.K. *et al.* Electronic Raman and infrared spectra of acceptors in isotopically controlled diamonds. *Phys. Rev. B*. 1998. **57**. P. 15315–15327. <https://doi.org/10.1103/PhysRevB.57.15315>.
18. Pruvost F., Bustarret E., Deneuve A. Characteristics of homoepitaxial heavily boron-doped diamond films from their Raman spectra. *Diam. Relat. Mater.* 2000. **9**. P. 295–299. [https://doi.org/10.1016/S0925-9635\(99\)00241-1](https://doi.org/10.1016/S0925-9635(99)00241-1).
19. Blank V.D., Denisov V.N., Kirichenko A.N. *et al.* Raman scattering by defect-induced excitations in boron-doped diamond single crystals. *Diam. Relat. Mater.* 2008. **17**. P. 1840–1843. <https://doi.org/10.1016/j.diamond.2008.07.004>.
20. Bernard M., Deneuve A., Muret P. Non-destructive determination of the boron concentration of heavily doped metallic diamond thin films from Raman spectroscopy. *Diam. Relat. Mater.* 2004. **13**. P. 282–286. <https://doi.org/10.1016/j.diamond.2003.10.051>.
21. Ushizawa K., Watanabe K., Ando T. *et al.* Boron concentration dependence of Raman spectra on {100} and {111} facets of B-doped CVD diamond. *Diam. Relat. Mater.* 1998. **7**. P. 1719–1722. [https://doi.org/10.1016/S0925-9635\(98\)00296-9](https://doi.org/10.1016/S0925-9635(98)00296-9).
22. Kovalenko T.V., Lysakovskiy V.V., Kvasnitsya V.M. *et al.* Morphology of diamond single crystals grown in the Fe-Co-Mg-C system. *J. Cryst. Growth*. 2019. **507**. P. 327–331. <https://doi.org/10.1016/j.jcrysgro.2018.11.040>.
23. Li R.F., Thomson G.B., White G. *et al.* Integration of crystal morphology modeling and on-line shape measurement. *AIChE J.* 2006. **52**. P. 2297–2305. <https://doi.org/10.1002/aic.10818>.
24. Raabe D., Sachtler M. Measurement of plastic strains by 3D image correlation photogrammetry at the grain scale, MPI für Eisenforschung GmbH, Düsseldorf, Germany, 2003. <http://hdl.handle.net/11858/00-001M-0000-0019-6B8A-F>.
25. Pajeroski D.M., Ng R., Peterson N. *et al.* 3D scanning and 3D printing AlSi10Mg single crystal mounts for neutron scattering. *Rev. Sci. Instrum.* 2020. **91**. P. 053902. <https://doi.org/10.1063/5.0008599>.
26. Ager J.W., Walukiewicz W., McCluskey M. *et al.* Fano interference of the Raman phonon in heavily boron-doped diamond films grown by chemical vapor deposition. *Appl. Phys. Lett.* 1995. **66**. P. 616–618. <https://doi.org/10.1063/1.114031>.
27. Tallaire A., Kasu M., Ueda K., Makimoto T. Origin of growth defects in CVD diamond epitaxial films. *Diam. Relat. Mater.* 2008. **17**. P. 60–65. <https://doi.org/10.1016/j.diamond.2007.10.003>.
28. Bormashov V.S., Tarelkin S.A., Buga S.G. *et al.* Electrical properties of the high quality boron-doped synthetic single-crystal diamonds grown by the temperature gradient method. *Diam. Relat. Mater.* 2013. **35**. P. 19–23. <https://doi.org/10.1016/j.diamond.2013.02.011>.
29. Blank V.D., Bormashov V.S., Tarelkin S.A. *et al.* Power high-voltage and fast response Schottky barrier diamond diodes. *Diam. Relat. Mater.* 2015. **57**. P. 32–36. <https://doi.org/10.1016/j.diamond.2015.01.005>.

#### Authors and CV



**Viktor V. Strelchuk.** Professor, Doctor of Physics. Head of Optical Submicron Spectroscopy Laboratory, V. Lashkaryov Institute of Semiconductor Physics, NASU. Field of research: physics of semiconductors, Raman and photoluminescence spectroscopy of semiconductors, nanostructures and nanoscale materials. He is the author of more than 100 science papers and technical patents.  
ORCID:0000-0002-6894-1742



**Andrii S. Nikolenko.** PhD, Senior Researcher at the Optical Submicron Spectroscopy Laboratory, V. Lashkaryov Institute of Semiconductor Physics, NASU. Field of research: semiconductor physics, semiconductor nanostructures and heterostructures, Raman, photoluminescence and FTIR spectroscopy. He is the author of more than 60 science papers and technical patents.  
ORCID:0000-0001-6775-3451  
E-mail: nikolenko@isp.kiev.ua



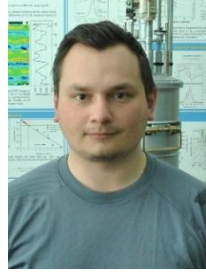
**Petro M. Lytvyn.** PhD in Physics and Mathematics, Senior Researcher of the Laboratory of electron probe methods of structural and elemental analysis of semiconductor materials and systems, V. Lashkaryov Institute of Semiconductor Physics, NASU. The area of scientific interests covers nanophysics of semiconductors and related materials.  
ORCID: 0000-0002-0131-9860  
E-mail:plyt2007@gmail.com



**Sergii O. Ivakhnenko.** Professor, Doctor of Technical Sciences, Corresponding member of NAS of Ukraine. The area of scientific interests covers phase transformations in elements and materials at high pressures and high temperatures, nucleation and growth kinetics of diamond single crystals in solution-melt systems at

high pressure and high temperature. He is the author of more than 300 science papers and technical patents.

E-mail: sioz@ismv13.kiev.ua



**Igor M. Danylenko.** PhD student of Optical Submicron Spectroscopy Laboratory, V. Lashkaryov Institute of Semiconductor Physics, NASU. The area of scientific interests covers Raman, PL and FTIR spectroscopy of semiconductors and nanostructures, optical, phonon and electrical properties of semiconductors and, in particular, of semiconducting diamond crystals.



**Tetiana V. Kovalenko.** PhD, Senior Researcher at V. Bakul Institute for Superhard Materials, NASU. The area of scientific interests covers: solution-melt crystallization of diamond at high pressures and temperatures, temperature gradient method, phase transformations at high pressures, semiconductors, morphology. She is the author of more than 60 science papers and technical patents.

E-mail: tetiana.v.kovalenko@gmail.com



**Sergii V. Malyuta.** PhD student of National Technical University of Ukraine "Igor Sikorsky Kyiv Polytechnic Institute". The area of scientific interests covers scanning probe microscopy (SPM), in particular, atomic force microscopy (AFM), Kelvin-probe force microscopy (KPFM), morphological properties of semiconductors and

nanostructures, diamond, SPM data processing and analysis.

ORCID: 0000-0003-0466-9900

E-mail: serhiy.malyuta@gmail.com

### Секторальна залежність морфологічних, структурних і оптичних властивостей легованих бором кристалів НРНТ алмазу

**В.В. Стрельчук, А.С. Ніколенко, П.М. Литвин, С.О. Івахненко, Т.В. Коваленко, І.М. Даниленко, С.В. Мalyюта**

**Анотація.** Леговані бором напівпровідникові монокристали алмазу кубооктаедричного габітусу з переважним розвитком граней октаедра {111} і незначною площею граней куба {001}, ромбододекаедра {110} і тетрагон-триоктаедра {311} було отримано методом розчин-розплавної кристалізації під високим тиском 6,5 ГПа і при температурах 1380...1420 °С. Використання розчинника Fe-Al, який дозволяє контролювати включення домішки бору у межах  $2 \cdot 10^{-4} \dots 10^{-2}$  ат.%, дало можливість варіювати електрофізичні властивості кристалів. Методи мікро-фотограмметрії, атомно-силової мікроскопії та мікро-раманівської спектроскопії були застосовані для виявлення секторальної неоднорідності домішкового складу і морфології різних граней кристалів. Показано, що отримані кристали мають високу структурну досконалість і концентрацію бору від  $\sim 1 \cdot 10^{17}$  до  $\sim 7 \cdot 10^{18}$  см<sup>-3</sup>. Збільшення концентрації бору призводить до зростання площі граней {111} у порівнянні із загальною площею кристала. Показано, що нанорозмірні морфологічні особливості, такі як тераси росту, сходинки, дендритоподібні наноструктури, стовпчасті субструктури, негативні піраміди росту на різних гранях кристала відображають особливості процесів розчинення вуглецю при високому тиску і високих температурах. Зміни габітусу і морфології поверхні кристалів обговорюються у зв'язку з неоднорідною зміною термодинамічних умов росту і розчинення граней кристалів при різних концентраціях бору.

**Ключові слова:** леговані бором кристали НРНТ алмазу, раманівська спектроскопія, атомно-силова мікроскопія, мікро-фотограмметрія.